

A Real-Time Electrically Controlled Active Matching Circuit Utilizing Genetic Algorithms for Wireless Power Transfer to Biomedical Implants

Jo Bito (美藤成), *Student Member, IEEE*, Soyeon Jeong, *Student Member, IEEE*, and Manos M. Tentzeris, *Fellow, IEEE*

Abstract—This paper discusses the feasibility of a real-time active matching circuit (MC) for wireless power transfer applications, especially for biomedical systems. One prototype of low-cost real-time automatic MC, utilizing a variable circuit topology, including discrete passives and p-i-n diodes, has been implemented and the principle has been verified by measurements. One genetic algorithm was introduced to optimize the design over a wide range of impedances to match. As a result of preliminary operation verification tests, the proposed real-time MC system results in improving the transfer coefficient in the range of 10–16-cm coil separation distance a maximum of 3.2 dB automatically in about 64 ms. Similar performance improvement results were observed in additional tests under misaligned conditions, as well as for nonsymmetrical Tx–Rx coil configurations further verifying the potential applicability of the proposed system to practical biomedical devices.

Index Terms—Autonomous sensors, genetic algorithms (GAs), impedance matching, real-time systems, wireless power transfer (WPT).

I. INTRODUCTION

WIRELESS power transfer (WPT) technology is one of the most highly demanded technologies to realize truly cableless/batteryless mobile devices and wirelessly connected electronics, which are required for practical implementations of Internet of Things (IoT) topologies, and could potentially alleviate the typical issues of the short cruising range until next recharging, as well as the inconvenience of wired charging of electrical vehicles [1]–[3]. In addition to these applications, the medical field is one of the most important application areas of this technology. For hygienic purposes, the unique capability of HF waves and microwaves to transfer power to sealed devices in a contactless/cableless way is a major advantage. Furthermore, WPT could have a significant impact in health and

biomonitoring applications, virtually eliminating the need for painful and infection-prone surgical procedures, which are currently necessary for periodical battery replacement, by wirelessly charging *in-vivo* implanted electronics.

Generally, there are three types of electromagnetic (EM) wireless power transmission systems: far-field radio waves, inductive power transfer, and capacitive power transfer—and each method has its pros and cons [4], [5]. The resonant coupling, especially the magnetic resonant coupling method, which belongs to the inductive power transfer techniques, has attracted the interest of the research community today because of its relatively large operation distance and high maximum power transmission efficiency [6]. Also, the magnetic coupling is preferred to satisfy the fundamental requirement of penetrating the human body, which is electrically lossy conductor, to provide the power to the receiver (Rx) in the human body. A two-frequency split, called the “horn effect,” is usually associated with the fundamental operation of the magnetic resonance wireless power transmission in configurations with very small separation distances between transmitter (Tx) and Rx coils [3]. This can be a major issue for WPT applications on moving or nonstationary platforms, such as the human body, typically pushing the values of the resonance frequency outside the allowable frequency bands or drastically deteriorating the coupling efficiency. In order to compensate for the effect of human body part movements (e.g., breathing and turning), a real-time active matching circuit (MC) has to be inserted between the signal source and the Tx coil. The overview of a typical magnetic resonant wireless power transmission system with real-time MCs on the Tx side is depicted in Fig. 1. As already reported, it is possible to design a discrete value MC with a combination of lumped circuit elements and p-i-n diode switches utilizing a genetic algorithm (GA). The MC is electrically controlled by a microcontroller to decrease the mismatch between the signal generator and the transmitting coil, which has the self-resonance frequency of 13.56 MHz [7]. In this paper, the implementation of an entire real-time active MC as well as further operation tests under different coil separation distances, practical misaligned conditions, and asymmetry coils configurations are discussed in detail as an extension of previously reported results.

Manuscript received July 16, 2015; revised November 08, 2015; accepted December 11, 2015. Date of publication January 18, 2016; date of current version February 03, 2016. The work of J. Bito, S. Jeong, and M. M. Tentzeris was supported by the National Science Foundation (NSF) and by the Defense Threat Reduction Agency (DTRA). This paper is an expanded version from the IEEE MTT-S Wireless Power Transfer Conference, Boulder, CO, USA, May 13–15, 2015.

The authors are with the School of Electrical and Computer Engineering, Georgia Institute of Technology, Atlanta, GA 30332-250 USA (e-mail: jbito3@gatech.edu).

Color versions of one or more of the figures in this paper are available online at <http://ieeexplore.ieee.org>.

Digital Object Identifier 10.1109/TMTT.2015.2513765

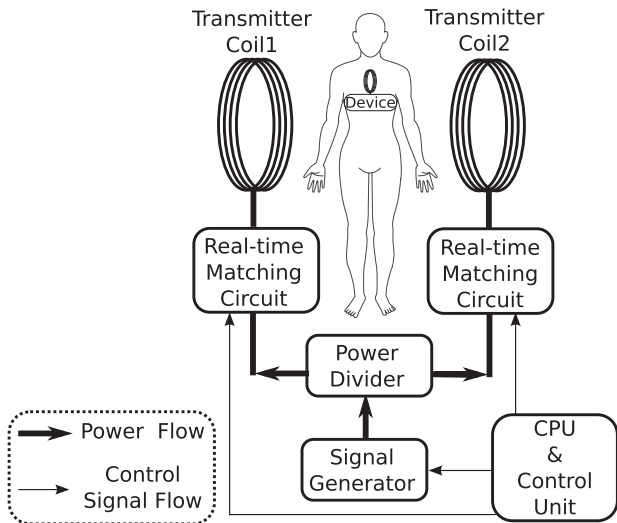


Fig. 1. Block diagram of a dual-transmitting-coil wireless power transmission system with on-Tx real-time MCs.

TABLE I
PARAMETERS OF THE OPTIMIZED OPEN-HELICAL-COIL
FOR THE PROPOSED WPT SYSTEM

Parameters	Values
Radius of coil	50 mm
Diameter of wire	1 mm
Gap between loops	0.2 mm
Number of turns	26
Height of coil	60 mm
Self-resonance frequency	13.56 MHz

II. TX AND RX COIL DESIGN

In order to confirm the transition from the strongly coupled regime to the weakly coupled regime in the small coil separation distance range, for proof-of-concept purposes and without loss of generality, an open type helical coil, which has the self-resonance frequency of 13.56 MHz, was designed on CST Studio Suite 2014 within the size restriction in the diameter of 10 cm. In the preliminary measurement setup, in order to simplify the experiments, the same coil design was adopted for both Tx and Rx coils. The extension of the presented approach to coils of different size is straightforward. During the simulation process, the gap between each coil wires was optimized to reduce the radiation loss in given specific fabrication limitations. In order to reduce the simulation time, the integral solver was adopted. The simulation results yielded the following coil dimensions as summarized in Table I; the radius of the coil is 50 mm, the diameter of the copper wire is 1 mm, the gap between consecutive turns is 0.2 mm, and the number of turns is 26, to achieve the operation frequency of 13.56 MHz. Based on the simulation results, the Tx and the Rx coil prototypes were fabricated with a 1-mm-diameter copper wire utilizing laser cut acrylic boards for support purposes. A photograph of the fabricated Tx and Rx coils, the simulated and the measured S_{11} values of the single coil without any other coil in its proximity, and the measured S_{21} value values for different center-to-center coil distances (identical Tx and Rx coils) are shown in Fig. 2(a)–(c), respectively.

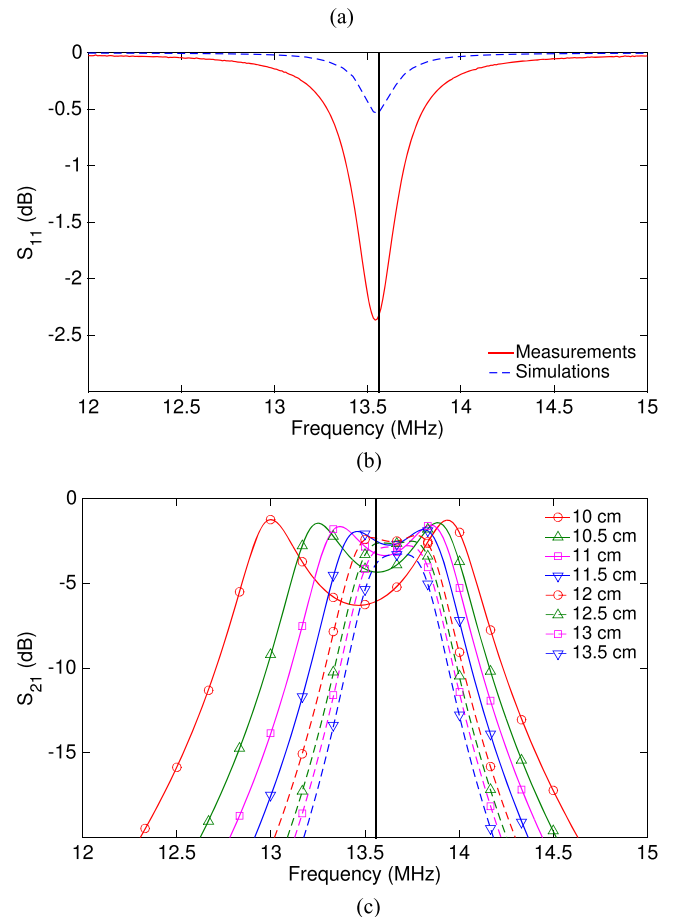
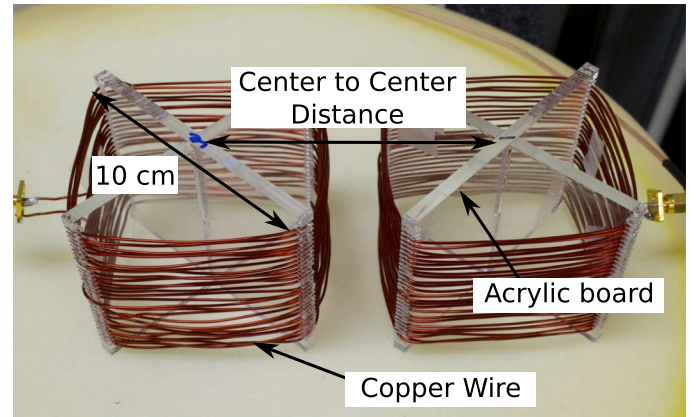


Fig. 2. (a) Open-helical-coil prototype for WPT system. (b) Measured and simulated S_{11} of the single open helical coil prototype. (c) Measured S_{21} of the open-helical-coil WPT coil network at different separation distances.

The higher loss in the measurement results is assumed to be associated with greater radiation loss because of the fabrication error, the conductor loss associated with the copper wires, and the dielectric loss because of the acrylic board supporters. As depicted in Fig. 2(c), two frequency peaks can be seen at coil separation distances up to 12 cm.

An open helical coil can be approximated with an equivalent series RLC circuit. If the resistance, the inductance and the capacitance of the single coil are R , L , and C , the impedance of the coil, Z_{in} , is given by (1), where ω is an angular frequency. Specifically, the imaginary part of the coil impedance,

X_{in} , can be expressed as shown in (2). Practically, the values of the self-inductance and of the self-capacitance of the coil remain constant over the frequency range of operation, allowing us to derive their values from the imaginary part of the measured coil impedance at two frequency points. If the mutual inductance between the two coupled coils is L_m , its value can be derived from the self-resonance frequency of the single coil, f_0 , and the upper and lower resonance frequency of two coupled (Tx and Rx) coils, f_u , f_l , using (3) [8], [9]. From the measurement data, the inductance and the capacitance of the open helical coil prototype have been derived to be equal to $21.8 \mu\text{H}$ and 6.34 pF , respectively. Also, the mutual inductance at 10-cm coil distance, for example, is $1.51 \mu\text{H}$,

$$Z_{in} = R + j \left(\omega L - \frac{1}{\omega C} \right) \quad (1)$$

$$X_{in} = \omega L - \frac{1}{\omega C} \quad (2)$$

$$L_m = \left(\frac{f_u^2 - f_l^2}{f_u^2 + f_l^2} \right) L. \quad (3)$$

III. MC DESIGN USING A GA

A. MC Design Process

In ideal cases, a dynamically changing MC can be easily implemented as a π network, which has variable component values. However, in reality, it is quite challenging to change the impedance values arbitrarily within a wide dynamic range using off-the-shelf components. There are various different ways to realize arbitrary different impedance values by utilizing electrically controlled variable circuit components, for example, by using relays [10] or varactor diodes [11]. However, in the research presented in this paper, a discrete value impedance MC with p-i-n diode switches is adopted because of its fast switching speed, small feature size, and robustness [12]. The MC topology is based on the cascading of a unit cell consisting of an L-type series inductor and shunt capacitor. The L-type topology was chosen to make the unit-cell configuration as simple as possible to minimize the simulation and the optimization time for MC design. Ideally, the range of impedance values created by the variable MC unit increases as the number of stages increases. However, in reality, this value range saturates at some point because of the discrete available circuit component values. At the same time, the loss associated with the lumped circuit components increases as the number of stage increases. Therefore, the number of stages (six in the prototype presented in this paper) was eventually chosen to satisfy the practical MC constraints described below with the minimum number of stages [7]. Each capacitor can be grounded through a p-i-n diode, which acts as the switching element. Since every switch provides two states, six switches can provide a total of 64 states. The p-i-n diodes are controlled by a microcontroller unit to choose the best configuration for the MC by changing the combination of “on” and “off” states of the p-i-n diodes. In this work, the p-i-n diode SMP1340 from Skyworks Solutions Inc. is adopted in order to achieve a high-speed MC operation. In this effort, a GA was utilized in order to determine the optimal lumped component

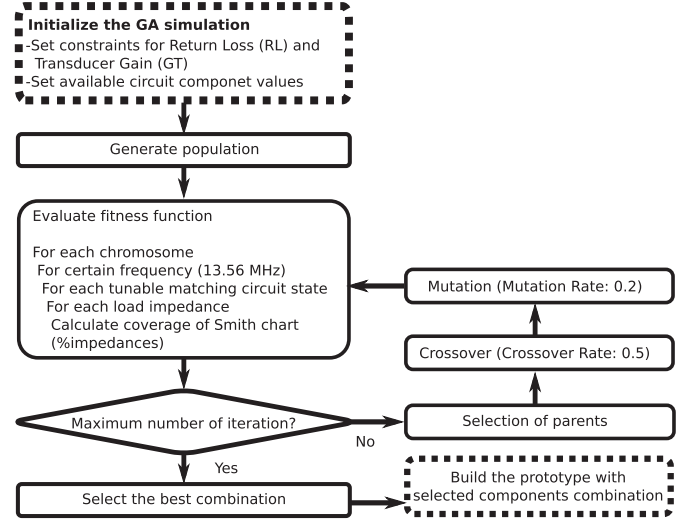


Fig. 3. Flowchart of the GA optimization for the MC design.

values for typical WPT matching applications out of the available standard “off-the-shelf” discrete component values aiming at achieving an effective matching over a large part of the Smith chart, virtually covering most impedance values to match in the practical WPT configurations.

GAs are heuristic search methods, which have been widely used to solve EM optimization problems [13]. Here, for the easy and quick implementation of GA into the MC design, the Global Optimization Toolbox of MATLAB was utilized. The procedure to design and to evaluate the performance of the MC is described in Fig. 3 [12]. In summary, the MATLAB code generates discrete load impedance values, which are evenly distributed around the center of the Smith chart, and check how well the MC at each on/off p-i-n diode combination can match these different impedance values to 50Ω or not. The return loss (R_L) and the transducer gain (G_T), which are expressed in (4) and (5), are used as the criteria to assess the performance of the MC. These can be expressed as a function of the two-port S-parameters, and the load reflection coefficient (Γ_L) [14]. The return loss indicates the quality of matching to the load impedance. This is a necessary condition to check if port1 (signal generator: 50Ω), is actually matched to port2 (Tx coil), which has an arbitrary impedance, or not. However, this condition is not a sufficient condition to guarantee the improvement in power transfer from port1 to port2 because there is a dissipative loss associated with the insertion of the MC and a load mismatch [15],

$$R_L = -20 \log \left(S_{11} + \frac{S_{12}S_{21}\Gamma_L}{1 - S_{22}\Gamma_L} \right) \quad (\text{dB}) \quad (4)$$

$$G_T = -10 \log \left(\frac{|S_{21}|^2 (1 - |\Gamma_L|^2)}{|1 - S_{22}\Gamma_L|^2} \right) \quad (\text{dB}). \quad (5)$$

From the literature, it is possible to achieve the maximum Smith chart coverage (up to 70%) under the conditions, $R_L < -10 \text{ dB}$ and $G_T > -2 \text{ dB}$, which guarantees the sufficient improvement of matching by utilizing arbitrary circuit component values [12]. The proposed method can effectively realize

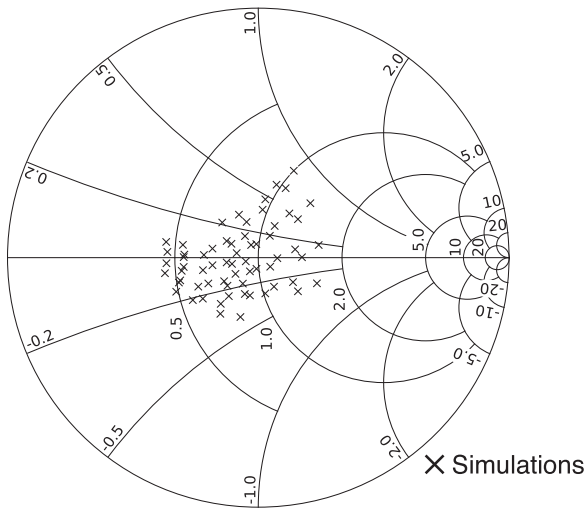


Fig. 4. Simulated input impedance values generated by MATLAB's GA algorithm.

a Smith chart coverage of 50%–60% satisfying the same criteria by modifying the combination of a discrete set of circuit components. Each component value in these sets is chosen from commercially available lumped component values. For both inductors and capacitors, 28 consecutive commonly used circuit values, which cover a lumped element value range of 1000:1 for the operation frequency of 13.56 MHz were considered. By limiting the number of components in the MC in such a way, the simulation time was significantly reduced.

B. Characterization of MC

During the GA simulations, based on the available lumped component values, the center of the Smith chart was targeted, offering a 50%–60% Smith chart coverage at 13.56 MHz. The input impedance values of the MC at each on/off state generated by MATLAB are shown in Fig. 4. However, the inductive component value of the fifth cell was changed from 27 to 560 nH through the simulations utilizing Advanced Design System (ADS) 2013 in order to fine tune the optimization process for the measured coil S-parameters. This improved the MC performance at the short coil separation distances, and eventually increased the range of coil separation distance that can be matched. In Fig. 5, the schematic of the GA-designed MC after the fine tuning and the picture of the MC prototype are depicted. The circuit prototype was fabricated on a 1.5-mm-thick substrate, RO4003C, which features a dielectric constant of 3.38, provided by the Rogers Cooperation. The measured and simulated reflection coefficient values for the designed MC after the fine tuning are shown in Fig. 6. During the measurements, bias circuits, each composed of a series inductor and a parallel capacitor, were connected to each pin of the MC prototype to isolate Arduino Uno microcontroller board's general input output pins (GIOPs), which provide the dc voltage for each p-i-n diode, from the rest of the matching network. As can be easily observed in Fig. 6, the simulation and the measurement results agree quite well.

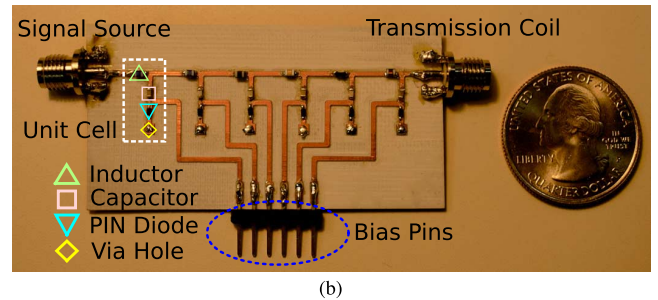
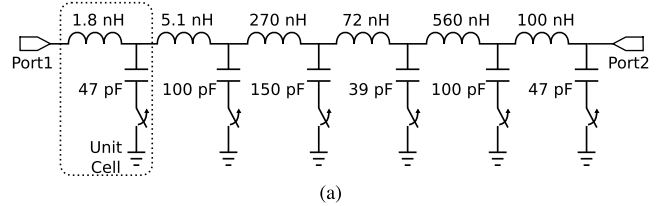


Fig. 5. (a) Tunable sixth-stage MC schematic derived using the GA and ADS. (b) Prototype of the tunable MC with modified components value.

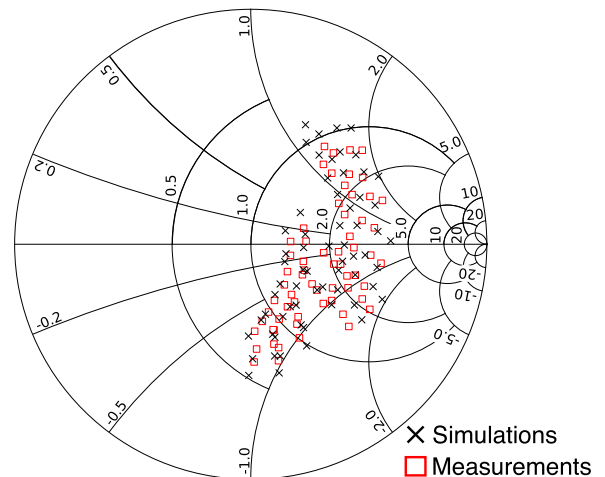


Fig. 6. Measured and simulated input impedance values of tunable MC prototype.

IV. REAL-TIME MC SYSTEM

One of the easiest and most accurate ways to assess the quality of the matching and operate the system at the maximum power transfer point is to monitor the S-parameters values and modify the configuration of the active MC in real time to achieve the highest value of the transmission coefficient (minimum reflection coefficient) for time-changing topologies. However, in reality, introducing a network analyzer into the system is not a practical choice in terms of cost and flexibility. Also, in practical implantable systems, it is virtually impossible to have a physical connection between the Rx device and the matching quality control unit, thus making it difficult to directly measure the received power. In order to overcome this problem, a maximum power to the Tx, that is measured by utilizing a directional coupler and an RF detector integrated circuit (IC), which is mainly composed of a detector diode, was designed as shown in Fig. 7. In this system, a fraction of the reflected signal from the Rx coil is fed through the coupled port of a directional coupler to a detector diode, and the output dc voltage from the

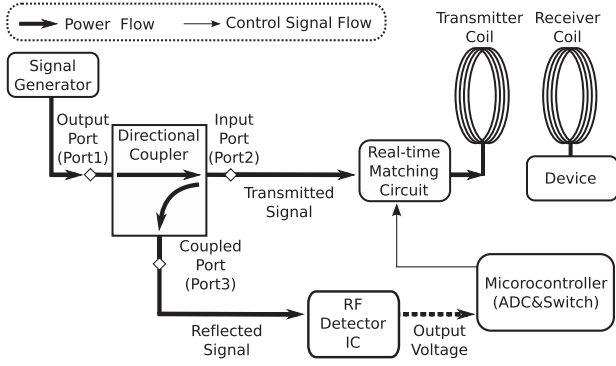
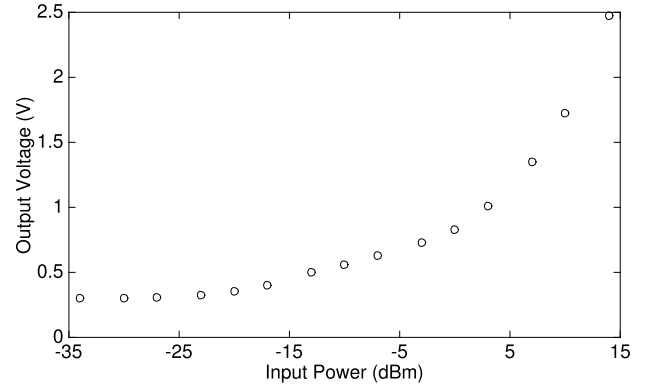


Fig. 7. Block diagram of an MC quality assessment system utilizing a directional coupler and an RF detector IC.

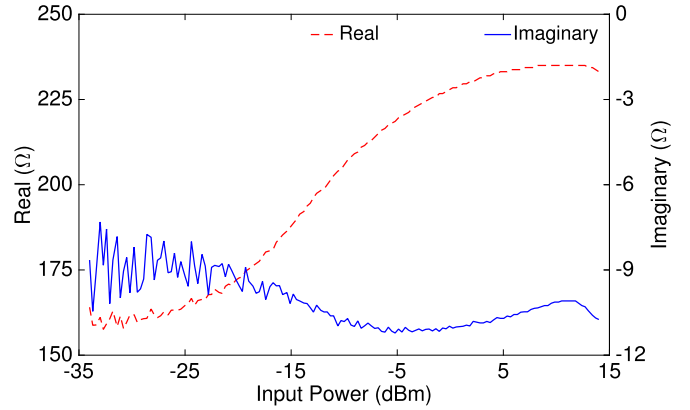
diode is measured by utilizing an analog-to-digital converter (ADC) in the microcontroller module. With this method, the system does not require any RF measurement equipment, which usually increases the system cost and complexity while limiting its applicability. If the output voltage of the detector diode is at the minimum value, it can be assumed that the reflection from the Tx coil is minimized, which equivalently means the highest power transmission in the ideal magnetic resonant Tx–Rx coil network.

A. Practical Limitations of Real-Time MC System

In practical implementations, due to the requirements for the optimal operation of directional coupler, as well as due to the performance characteristics of the detector diodes, there exist numerous fundamental system limitations. The efficient operation of the directional couplers is guaranteed only when all their ports are matched [16]. Therefore, if the active MC cannot sufficiently match the Tx coil to the directional coupler, the reflected power estimation is no longer accurate, while the insertion loss of the directional coupler increases. In addition, the impedance of commercial detection diodes strongly depend on the input power level, thus drastically affecting the system performance. In the proof-of-concept prototype presented in this paper, the -15 -dB directional coupler, ZEDC-15-2B from Mini-Circuits, and the RF detector IC, LTC5507 from the Linear Technology Cooperation, were used. In order to identify the practical system limitations, the output voltage and the impedance of the RF detector IC were measured for different input power levels within the range from -34 to 14 dBm with values plotted in Fig. 8. As a result, it can be said that the RF detector IC covers a quite wide dynamic range of input power levels providing an easily detectable output voltage change. The real part of input impedance varies from about 160 to 230Ω depending on the input power level, and the imaginary part of the impedance is almost constant around -10Ω . Next, based on these measured values, the effect of the directional coupler on the system performance was investigated through simulations on ADS by using the measured S-parameters of the coupler. For convenience, the output port, the input port, and the coupled port of the directional coupler are named port1, port2, and port3, respectively. In the actual real-time matching system, port1, which is connected to the



(a)



(b)

Fig. 8. (a) Measured output voltage from the RF detector IC with respect to the input power. (b) Measured impedance of the RF detector with respect to the input power.

signal generator, is assumed to be always matched. Therefore, the S-parameters of the coupler were simulated by changing the impedance of port2 and port3. After performing numerous simulations, it was observed that the impedance change at port3 over the above measured range of the impedance variation of the detector IC does not significantly affect the S-parameters of the coupler. However, the impedance mismatch at port2 drastically changes the S-parameters. Fig. 9(a) and (b) shows the values of S_{21} and S_{32} of the coupler when the real and the imaginary parts of the terminal impedance at port2 were varied from 20 to 130Ω and from 0 to 200Ω , respectively, by assuming that this is the change of input impedance of the Tx coil caused by the coil separation distance change. As it can be easily concluded from the numerical simulations shown in Fig. 9(a), the insertion loss increases as the mismatch at port2 increases. For a practical system implementation, up to 1 dBm worsening of the matching performance, which is equivalently from 20 to 130Ω , must be satisfied to guarantee the effective system performance. At the same time, Fig. 9(b) implies that there is an undetectable region near the perfectly matched condition because of too low reflected power below -34 dBm, which is the lower boundary of the detectable RF signal utilizing the RF detector IC. Although, if this happens or not depends on the level of input power to the system, in general.

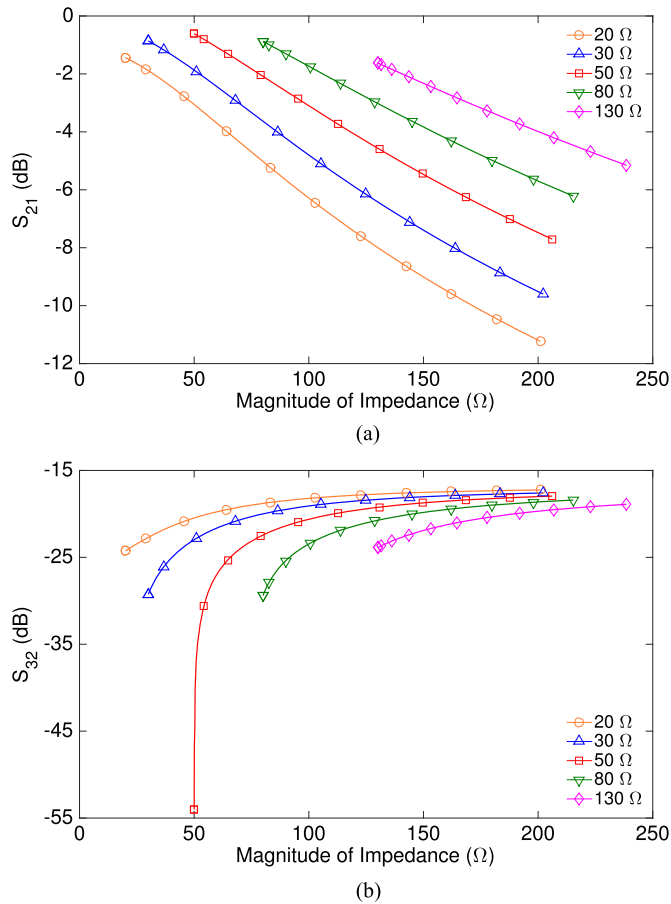


Fig. 9. (a) S_{21} of the directional coupler for different terminal impedance values of port2. (b) S_{32} of the directional coupler for different terminal impedance values of port2.

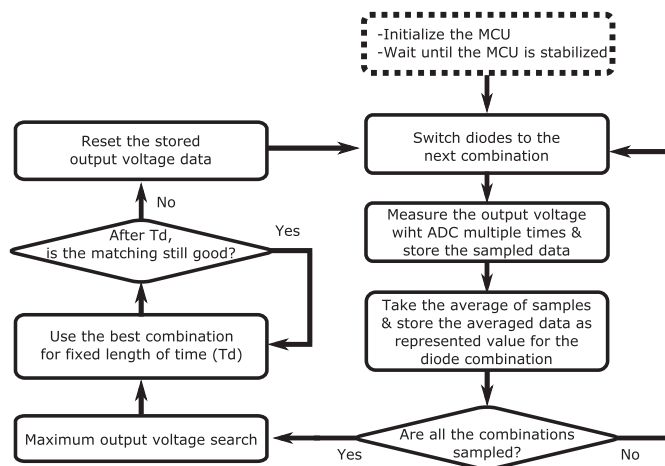


Fig. 10. Flowchart of the automated real-time matching procedure utilizing a microcontroller.

B. Automated Real-Time Maximum Power Transfer Point Search

Based on the assumption that the lowest output voltage from the RF detector IC is correlated to the highest transferred power, the brute force real-time matching algorithm, as shown in Fig. 10, was implemented by utilizing a microcontroller module, Arduino Uno. The major limitations for a fast real-time

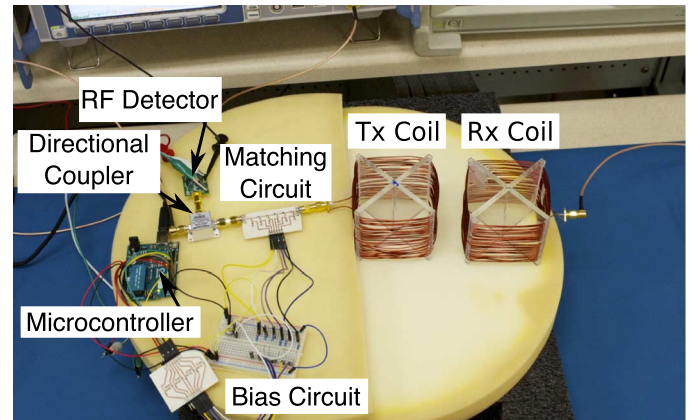


Fig. 11. Complete setup of the automated real-time matching system for operation testing purposes.

MC operation are the switching speed of the p-i-n diode and the reading rate of the ADC in the microcontroller. From the datasheet, the switching time of p-i-n diode in our system prototype, SMP1340, is in the range of hundreds of nanoseconds [17], [18]. However, the maximum reading rate of the ADC in Arduino is about 10 kHz. In our MC prototype, there are 64 states by using six p-i-n diodes. Therefore, the minimum required time for the matching is about 6.4 ms by taking only one ADC measurement for each state. In actual operation tests, ten measurements are conducted for each state for enhanced smoothing in order to increase the measurement accuracy. Therefore, the expected required time for the optimum operation point search is about 64 ms. Ideally, the required time can be reduced by introducing fast ADCs potentially reducing the time to less than 1 ms. By taking into account the fast switching time of the p-i-n diode, the time for matching can be less than 1 ms.

V. OPERATION TEST OF THE AUTOMATED REAL-TIME MATCHING SYSTEM

A. Performance Characterization of Automated Real-Time Matching System

In order to test the performance of the developed automated real-time matching system, all the components are arranged as shown in Fig. 11, and the received power at different separation distances was measured by utilizing a real-time spectrum analyzer, RSA3408A from Tektronix Inc., with and without an MC. The input power to the MC and the Tx coil is adjusted to be 0 dBm in both cases with and without a MC, respectively. The received power with respect to the coil center to center separation distance with and without an automated matching system is depicted in Fig. 12. It can be easily concluded that the received power increases by utilizing the MC for separation distances in the range from 10 to 16 cm with a maximum received power improvement of 3.2 dB. In order to specify the quality of the real-time MC, the S_{11} of the Tx-Rx coil network with and without an MC operating at the best/optimum performance state automatically chosen by the microcontroller at different coil separation distance are measured by using a vector network

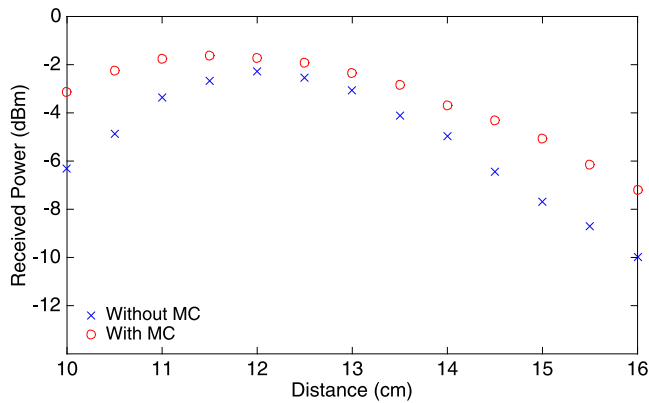


Fig. 12. Measured received power with and without the automated MC at different coil separation distances.

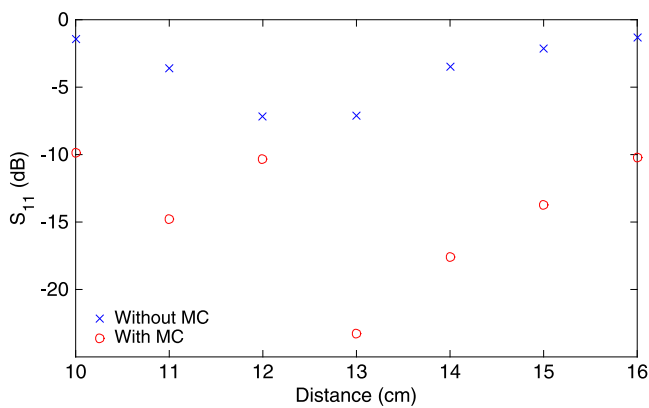


Fig. 13. Measured S_{11} of coil with and without the MC at the optimal power transfer state that is automatically chosen by the microcontroller at different coil separation distances.

analyzer, ZVA8 from Rohde & Schwarz, and results are shown in Fig. 13. After 16 cm, there is no significant change in S_{11} for both with and without MC cases. Since the diameter of the coil is 10 cm and it is the minimum possible center to center separation distance between two coils, the coil's matching is improved over the entire separation distance range from 10 to 16 cm or more.

Finally, the output voltage from the detector IC and the received power are measured at different coil separation distances by changing the configuration of the MC by manually turning on/off the switches to emulate all possible states in order to confirm whether the automated MC is actually choosing the optimal combination of on/off states or not. The received power at 10, 12, 14.5, and 16 cm are shown in Fig. 14(a)–(d), respectively. From the figures, it can be said that, at 12 cm, the voltage reading of microcontroller is not accurate because of the too low reflected power associated with the good matching, as previously explained in the section of the system limitation. This can be the reason why the S_{11} is high at 12 cm in Fig. 13. This can be prevented by using a coupler, which has a high coupling coefficient or the input power to the system is high. Similarly, at 16 cm, the high mismatch at the input port of the coupler breaks the correlation of low reflected power and high transferred power, and the automated MC cannot choose the best combination from the

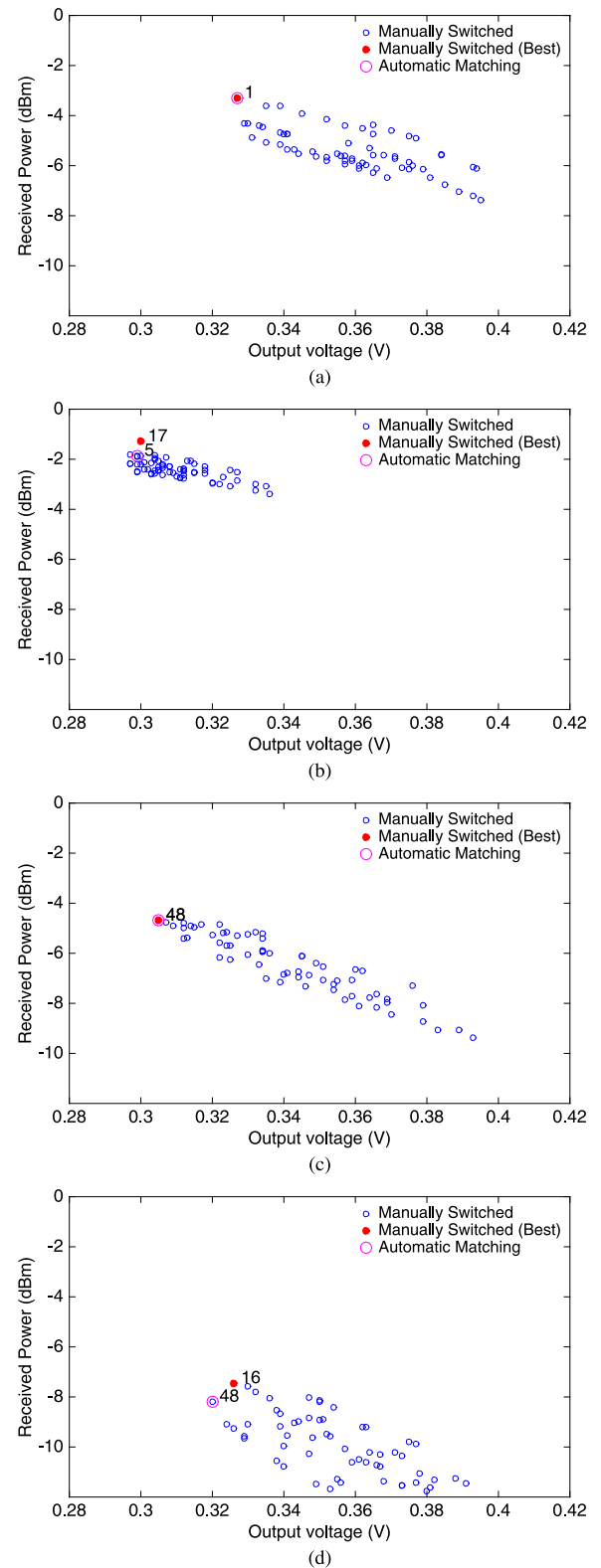


Fig. 14. Measured received power from the Rx coil and the output voltage from the RF detector IC at each p-i-n diode on/off state with coil separation distance of: (a) 10 cm, (b) 12 cm, (c) 14.5 cm, and (d) 16 cm.

readout voltage data anymore. Therefore, technically 10–16 cm is the operation range of automated real-time matching system, although the variable MC unit can cover the entire separation distance range.

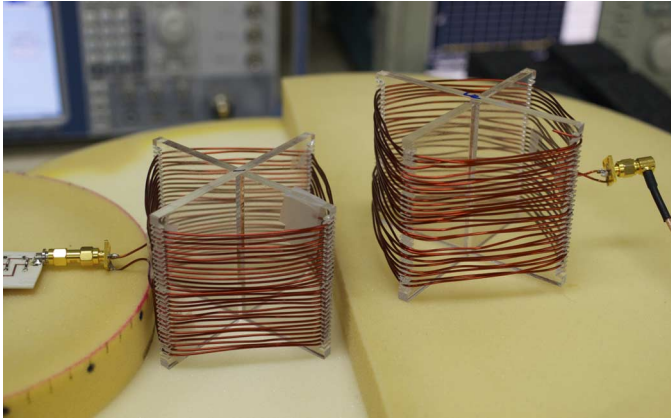


Fig. 15. Tx–Rx coil network under misaligned conditions caused by relative elevation.

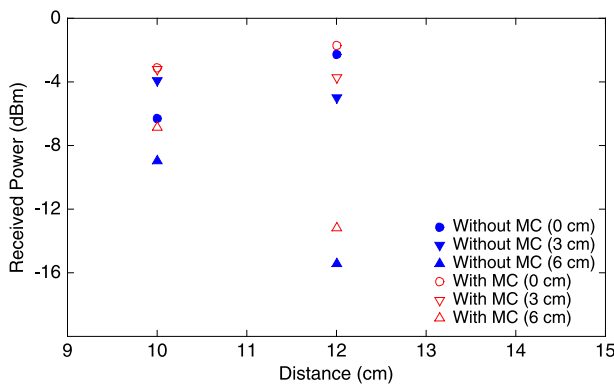


Fig. 16. Measured received power as a function of the coil separation distance for different Rx coil elevation levels.

B. Operation Tests Under Rugged Conditions

1) *Misalignment*: One of the fundamental motivations for this research was to create a real-time MC system, which can compensate the effect of human movements for Tx–Rx coil networks in practical biomedical WPT systems. One of the potential causes for the change of the Tx input impedance is the resulting Tx–Rx misalignment. Due to the geometrical symmetry of the designed coil, the effect of the misalignment in 2-D radial direction can be assumed to be limited. Therefore, in order to examine the capability of our real-time matching system to handle the misalignment, the received power with and without the MC was measured for misaligned positions caused by changing the elevation of the Rx coil. The Tx–Rx coil network setup testing the effect of the misalignment is shown in Fig. 15, and the received power with respect to the coil separation distance at different Rx coil elevations is depicted in Fig. 16. From these measurements, it appears that the automated real-time MC system can improve the power transfer at all data points, implying the potential matching capability of our system in 3-D coil movement.

2) *Nonsymmetrical Tx–Rx Coil Network*: Most biomedical WPT systems are expected to feature nonsymmetrical Tx–Rx coil topologies to increase the power transfer efficiency under the strict size constraints for the implantable Rx coils [19].

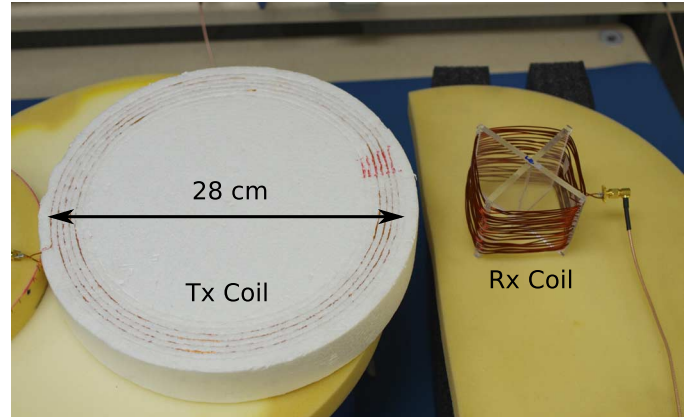


Fig. 17. Nonsymmetrical WPT coil system with a large Tx coil and a small Rx coil.

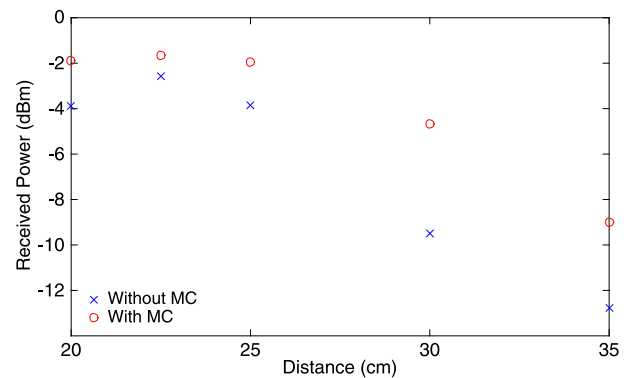


Fig. 18. Measured received power of the nonsymmetrical Tx–Rx coil network with respect to the coil separation distance.

Therefore, in order to further investigate the potential of the automated real-time matching system for biomedical applications, additional operation tests using nonsymmetrical Tx–Rx coil networks were conducted. For proof-of-concept purposes and without loss of generality, a larger planar loop open helical coil was utilized as the Tx coil. The minimum and the maximum radii of the coil loop are 12 and 14 cm, respectively, the diameter of the copper wire is 1 mm, the gap between the planar loop is 4 mm, and the number of turns is 5 for the Tx coil. A polystyrene foam was utilized as the supporting material for this coil, and the self-resonance frequency of the coil is 13.7 MHz. The slight self-resonance frequency shift from the expected operation frequency of 13.56 MHz was caused by the fabrication errors. The nonsymmetrical Tx–Rx coil testing setup is shown in Fig. 17, and the received power with respect to the coil separation distance is depicted in Fig. 18. As a result, the improvement in the received power was confirmed in the entire range from 20 cm or more. By introducing the larger Tx coil, the edge-to-edge coil separation distance range, which achieves a certain received power level, for example, above -3 dBm, increased compared to the symmetrical small Tx–Rx coil network. These preliminary promising results suggest the potential applicability of the proposed automated real-time matching system to nonsymmetrical WPT systems in biomedical implants.

VI. CONCLUSION

In this study, the feasibility of a real-time active MC for biomedical WPT applications is discussed. First, open helical type coils, which have a self-resonance frequency of 13.56 MHz, were designed utilizing an EM simulator and characterized through measurements. Based on the measured S-parameters of the coils, a variable MC unit was designed utilizing the GA. The prototype of low-cost real-time automatic MC was also designed and analyzed to quantitatively reveal the limitation of the real-time automatic matching system. Finally, the real-time matching system was implemented and verified through the measurement. Eventually, the proposed real-time automatic MC system achieved the maximum of 3.2-dB transfer coefficient improvement in the range of 10–16-cm coil separation distance automatically in about 64 ms. Additional operation verification tests conducted for misaligned coil topologies and for nonsymmetrical Tx–Rx WPT systems featured similar improvement results with the preliminary well-aligned same-size Tx and Rx configurations. These very promising preliminary results suggest the wide potential applicability of the proposed real-time automatic matching system to a variety of WPT applications, especially when there is strong coupling between Tx and Rx coil causing the frequency split, for example, charging of skin implanted devices, electrical vehicles, and unmanned aerial vehicles (UAVs). Possibly, the system can be applied to the powering of deep tissue implanted devices utilizing optimally designed coils.

REFERENCES

- [1] S. Kim *et al.*, “Ambient RF energy-harvesting technologies for self-sustainable standalone wireless sensor platforms,” *Proc. IEEE*, vol. 102, no. 11, pp. 1649–1666, Nov. 2014.
- [2] J. Shin, “Design and implementation of shaped magnetic-resonance-based wireless power transfer system for roadway-powered moving electric vehicles,” *IEEE Trans. Ind. Electron.*, vol. 61, no. 3, pp. 1179–1192, Mar. 2014.
- [3] T. Imura, H. Okabe, and Y. Hori, “Basic experimental study on helical antennas of wireless power transfer for electric vehicles by using magnetic resonant couplings,” in *IEEE Veh. Power Propulsion Conf.*, Dearborn, MI, USA, Sep. 2009, pp. 936–940.
- [4] H. Shoki, “Issues and initiatives for practical deployment of wireless power transfer technologies in japan,” *Proc. IEEE*, vol. 101, no. 6, pp. 1312–1320, Jun. 2013.
- [5] J. Dai and D. C. Ludois, “A survey of wireless power transfer and a critical comparison of inductive and capacitive coupling for small gap applications,” *IEEE Trans. Power Electron.*, vol. 30, no. 11, pp. 6017–6029, Nov. 2015.
- [6] A. Kurs, A. Karalis, R. Moffatt, J. D. Joannopoulos, P. Fisher, and M. Soljaj, “Wireless power transfer via strongly coupled magnetic resonances,” *Science*, vol. 317, no. 5834, pp. 83–86, Jul. 2007.
- [7] J. Bito, J. Soyeon, and M. M. Tentzeris, “A real-time electrically controlled active matching circuit utilizing genetic algorithms for biomedical WPT applications,” in *IEEE Wireless Power Transfer Conf.*, Boulder, CO, USA, May 2015, pp. 1–4.
- [8] T. Imura, H. Okabe, T. Uchida, and Y. Hori, “Study on open and short end helical antennas with capacitor in series of wireless power transfer using magnetic resonant couplings,” in *35th Annu. IEEE Ind. Electron. Soc. Conf.*, Porto, Portugal, Nov. 2009, pp. 3848–3853.
- [9] T. Imura and Y. Hori, “Maximizing air gap and efficiency of magnetic resonant coupling for wireless power transfer using equivalent circuit and neumann formula,” *IEEE Trans. Ind. Electron.*, vol. 58, no. 10, pp. 4746–4752, Oct. 2011.

- [10] T. C. Beh, M. Kato, T. Imura, S. Oh, and Y. Hori, “Automated impedance matching system for robust wireless power transfer via magnetic resonance coupling,” *IEEE Trans. Ind. Electron.*, vol. 60, no. 9, pp. 3689–3698, Sep. 2013.
- [11] H. M. Nemati, C. Fager, U. Gustavsson, R. Jos, and H. Zirath, “Design of varactor-based tunable matching networks for dynamic load modulation of high power amplifiers,” *IEEE Trans. Microw. Theory Techn.*, vol. 57, no. 5, pp. 1110–1118, May 2009.
- [12] C. Sanchez-Perez, J. de Mingo, P. L. Carro, and P. Garcia-Ducar, “Design and applications of a 300–800 MHz tunable matching network,” *IEEE Trans. Emerg. Sel. Topics Circuits Syst.*, vol. 3, no. 4, pp. 531–540, Dec. 2013.
- [13] J. M. Johnson and V. Rahmat-Samii, “Genetic algorithms in engineering electromagnetics,” *IEEE Antennas Propag. Mag.*, vol. 39, no. 4, pp. 7–21, Aug. 1997.
- [14] C. Sanchez-Perez, J. de Mingo, P. Garcia-Ducar, P. L. Carro, and A. Valdovinos, “Figures of merit and performance measurements for RF and microwave tunable matching networks,” in *Eur. Microw. Integr. Circuits Conf.*, Manchester, U.K., Oct. 2011, pp. 402–405.
- [15] F. Casini, R. V. Gatti, V. Perrone, and R. Sorrentino, “A new approach to the analysis and synthesis of lossy reconfigurable matching networks,” in *Proc. 39th Eur. Microw. Conf.*, Rome, Italy, Sep. 2009, pp. 1235–1238.
- [16] D. M. Pozar, *Microwave Engineering*, 4th ed. Hoboken, NJ, USA: Wiley, 2011.
- [17] “Design with PIN diodes,” Skyworks Solutions Inc., Woburn, MA, USA, Appl. Note, Oct. 2012.
- [18] “Fast switching speed, low capacitance, plastic packaged PIN diodes,” Skyworks Solutions Inc., Woburn, MA, USA, Data Sheet SMP1340 series, Jun. 2012.
- [19] A. K. RamRakhyani, S. Mirabbasi, and M. Chiao, “Design and optimization of resonance-based efficient wireless power delivery systems for biomedical implants,” *IEEE Trans. Biomed. Circuits Syst.*, vol. 5, no. 1, pp. 48–63, Feb. 2011.



Jo Bito (S'13) received the B.S. degree in electrical and electronic engineering from Okayama University, Okayama, Japan, in 2013. From 2010 to 2011, he joined the international programs in engineering (IPENG) and studied at the University of Illinois at Urbana–Champaign, Champaign, IL, USA. He is currently working toward the Ph.D. degree in electrical and computer engineering at the Georgia Institute of Technology, Atlanta, GA, USA.

He is currently a Research Assistant with the Agile Technologies for High-performance Electromagnetic Novel Applications (ATHENA) Group, Georgia Institute of Technology. His research interests include the application of inkjet printing technology for flexible and wearable electronics, RF energy harvesting, and wireless power transfer systems.

Mr. Bito was a recipient of the Japan Student Services Organization (JASSO) Long Term Scholarship beginning in 2013.



Soyeon Jeong (S'14) was born in Seoul, Korea. She received the Bachelor of Engineering degree in electrical engineering from Gangneung-Wonju National University, Kangwon, Korea, in 2010, the Master of Engineering degree in electrical and computer engineering from Georgia Institute of Technology, Atlanta, GA, USA, in 2014, and is currently working toward the Ph.D. degree at the Georgia Institute of Technology.

She is currently with the Agile Technologies for High-performance Electromagnetic Novel Applications (ATHENA) Group, Georgia Institute of Technology. Her current research is focused on wireless power transfer on methods, sensor component design, high-frequency characterization and environmental testing to the design, and simulation and fabrication of the RF system embedding the sensor.



Manos M. Tentzeris (S'89–M'92–SM'03–F'10) received the Diploma degree in electrical and computer engineering (*magna cum laude*) from the National Technical University of Athens, Athens, Greece, and the M.S. and Ph.D. degrees in electrical engineering and computer science from the University of Michigan, Ann Arbor, MI, USA.

He is currently a Professor with the School of Electrical and Computer Engineering, Georgia Institute of Technology, Atlanta, GA, USA. He currently heads the Agile Technologies for High-performance

Electromagnetic Novel Applications (ATHENA) Group, Georgia Institute of Technology (20 researchers). He has served as the Head of the Georgia Tech Electrical and Computer Engineering (GT-ECE) Electromagnetics Technical Interest Group, the Georgia Electronic Design Center Associate Director for RF identification (RFID)/sensors research (2006–2010), and the Georgia Institute of Technology National Science Foundation (NSF) Packaging Research Center Associate Director for RF Research and the RF Alliance Leader (2003–2006). He has helped develop academic programs in highly integrated/multilayer packaging for RF and wireless applications using ceramic and organic flexible materials, paper-based RF identifications (RFIDs) and sensors, biosensors, wearable electronics, 3-D/4-D/inkjet-printed electronics, “Green” electronics, energy harvesting and wireless power transfer systems, near-field communication (NFC) systems, nanotechnology applications in RF, origami-folded electromagnetics, microwave microelectromechanical systems (MEMs), system-on-package (SOP)-integrated (ultra-wideband (UWB), multiband, and millimeter-wave (mmW), conformal) antennas. During the summer of 2002, he was a Visiting Professor with the Technical University of Munich, Munich, Germany. During the summer of 2009, he was a Visiting Professor with GTRI-Ireland, Athlone, Ireland. During the summer of 2010, he was a Visiting Professor with LAAS-CNRS, Toulouse, France. He has authored or coauthored more than 550 papers in refereed journals and conference proceedings, 5 books, and 23 book chapters. He has given more than 100 invited talks to various universities and companies all over the world.

Dr. Tentzeris is a Member of URSI-Commission D. He is a Member of the MTT-15 Committee. He is an Associate Member of the European Microwave Association (EuMA). He is a Fellow of the Electromagnetic Academy. He is a

Member of the Technical Chamber of Greece. He served as an IEEE MTT-S Distinguished Microwave Lecturer (2010–2012). He is currently the IEEE C-RFID Distinguished Lecturer. He was the Technical Program Committee (TPC) Chair for the 2008 IEEE Microwave Theory and Techniques Society (IEEE MTT-S) International Microwave Symposium (IMS) and the Chair of the 2005 IEEE CEM-TD Workshop. He is the Vice-Chair of the RF Technical Committee (TC16), IEEE Components, Packaging, and Manufacturing Technology (CPMT) Society. He is the founder and chair of the RFID Technical Committee (TC24) of the IEEE MTT-S and the Secretary/Treasurer of the IEEE C-RFID. He is an Associate Editor for the IEEE TRANSACTIONS ON MICROWAVE THEORY AND TECHNIQUES, the *IEEE Transactions on Advanced Packaging*, and the *International Journal on Antennas and Propagation*. He was the recipient or corecipient of the 2015 IET Microwaves, Antennas and Propagation Premium Award, the 2014 Georgia Institute of Technology ECE Distinguished Faculty Achievement Award, the 2014 IEEE RFID-TA Best Student Paper Award, the 2013 IET Microwaves, Antennas, and Propagation Premium Award, the 2012 FiDiPro Award (Finland), the iCMG Architecture Award of Excellence, the 2010 IEEE Antennas and Propagation Society Piergiorgio L. E. Uslenghi Letters Prize Paper Award, the 2011 International Workshop on Structural Health Monitoring Best Student Paper Award, the 2010 Georgia Institute of Technology Senior Faculty Outstanding Undergraduate Research Mentor Award, the 2009 IEEE TRANSACTIONS ON COMPONENTS AND PACKAGING TECHNOLOGIES Best Paper Award, the 2009 E. T. S. Walton Award of the Irish Science Foundation, the 2007 IEEE Antennas and Propagation Society (AP-S) Symposium Best Student Paper Award, the 2007 IEEE MTT-S IMS Third Best Student Paper Award, the 2007 ISAP 2007 Poster Presentation Award, the 2006 IEEE MTT-S Outstanding Young Engineer Award, the 2006 Asia-Pacific Microwave Conference Award, the 2004 IEEE TRANSACTIONS ON ADVANCED PACKAGING Commendable Paper Award, the 2003 NASA Godfrey “Art” Anzic Collaborative Distinguished Publication Award, the 2003 IBC International Educator of the Year Award, the 2003 CPMT Outstanding Young Engineer Award, the 2002 International Conference on Microwave and Millimeter-Wave Technology Best Paper Award (Beijing, China), the 2002 Georgia Institute of Technology ECE Outstanding Junior Faculty Award, the 2001 ACES Conference Best Paper Award, the 2000 NSF CAREER Award, and the 1997 Best Paper Award of the International Hybrid Microelectronics and Packaging Society.